

1 **Topographical estimation of visual population receptive fields by fMRI**

2  
3 **Authors:**

4 Sangkyun Lee, Amalia Papanikolaou, Georgios A. Keliris, Stelios M. Smirnakis

5  
6 **Affiliation(s) for authors:**

7 Sangkyun Lee

8 Department of Neuroscience and Neurology, Baylor College of Medicine, Houston,  
9 TX 77030 USA

10 lee.sangkyun@gmail.com

11  
12 Amalia Papanikolaou

13 Max Planck Institute for Biological Cybernetics, Spemannstr. 38, 72076 Tübingen,  
14 Germany

15 amalia.papanikolaou@tuebingen.mpg.de

16  
17 Georgios A. Keliris

18 Max Planck Institute for Biological Cybernetics, Spemannstr. 38, 72076 Tübingen,  
19 Germany

20 Bernstein Center for Computational Neuroscience, Tübingen, Germany

21 georgios.keliris@tuebingen.mpg.de

22  
23 Stelios M. Smirnakis

24 Department of Neuroscience and Neurology, Baylor College of Medicine, Houston,  
25 TX 77030 USA

26 ssmirnakis@cns.bcm.edu

27  
28 **Corresponding author:**

29 Sangkyun Lee, Ph.D.

30 lee.sangkyun@gmail.com

31  
32 **Keywords:** population receptive field, vision, functional magnetic resonance imaging,  
33 retinotopy

34  
35 **Short Abstract:**

36 It is important to obtain unbiased estimates of visual population receptive fields  
37 (pRFs) by functional magnetic resonance imaging. We use mild regularization  
38 constraints to estimate pRF topography without a-priori assumptions about pRF

39 shape, allowing us to choose specific pRF models post-hoc. This is particularly  
40 advantageous in subjects with visual-pathway lesions.

41

## 42 **Long Abstract:**

43 Visual cortex is retinotopically organized so that neighboring populations of cells map  
44 to neighboring parts of the visual field. Functional magnetic resonance imaging  
45 allows us to estimate voxel-based population receptive fields (pRF), i.e., the part of  
46 the visual field that activates the cells within each voxel. Prior, direct, pRF estimation  
47 methods<sup>1</sup> suffer from certain limitations: 1) the pRF model is chosen a-priori and may  
48 not fully capture the actual pRF shape, and 2) pRF centers are prone to  
49 mislocalization near the border of the stimulus space. Here a new topographical pRF  
50 estimation method<sup>2</sup> is proposed that largely circumvents these limitations. A linear  
51 model is used to predict the Blood Oxygen Level-Dependent (BOLD) signal by  
52 convolving the linear response of the pRF to the visual stimulus with the canonical  
53 hemodynamic response function. PRF topography is represented as a weight vector  
54 whose components represent the strength of the aggregate response of voxel  
55 neurons to stimuli presented at different visual field locations. The resulting linear  
56 equations can be solved for the pRF weight vector using ridge regression<sup>3</sup>, yielding  
57 the pRF topography. A pRF model that is matched to the estimated topography can  
58 then be chosen post-hoc, thereby improving the estimates of pRF parameters such  
59 as pRF-center location, pRF orientation, size e.t.c. Having the pRF topography  
60 available also allows the visual verification of pRF parameter estimates allowing the  
61 extraction of various pRF properties without having to make a-priori assumptions  
62 about the pRF structure. This approach promises to be particularly useful for  
63 investigating the pRF organization of patients with disorders of the visual system.

64

## 65 **Introduction**

66 Functional magnetic resonance imaging (fMRI) measures non-invasively the  
67 functional organization of visual cortex at a macroscopic scale (typically on the order  
68 of millimeters). Early fMRI retinotopy studies used a coherence measure between  
69 stimulus location and elicited BOLD responses<sup>4-7</sup>. These studies typically did not  
70 estimate population receptive field size. Later, Dumoulin and Wandell<sup>1</sup> proposed a  
71 method to overcome such a limitation by explicitly modeling the pRF location and  
72 size, using a linear function of this model to predict the BOLD response. However,  
73 one limitation of this pioneering method is that the parametric pRF model has to be  
74 chosen a-priori, and may lead to erroneous pRF estimates if it turns out not to be  
75 appropriate.

76 To overcome limitations of the parametric pRF-model method, new methods have

77 been developed recently. These methods directly predict the BOLD response to the  
78 stimulus by reconstructing the pRF topography. A method<sup>8</sup> proposed by Greene and  
79 colleagues reconstructs the pRF topography by back-projecting the BOLD responses  
80 to the individual 1D stimulus spaces and building the pRF topography in the 2D  
81 stimulus space like a typical computer tomography technique. On the other hand, the  
82 method<sup>2</sup> proposed by us directly estimates the 2D pRF topography by using linear  
83 regression and applying a regularization technique. In this method, the pRF  
84 topography is represented as a set of weights which is multiplied by the stimulus to  
85 estimate the neuronal population response of a given voxel. Then, the final Blood  
86 Oxygen Level-Dependent (BOLD) response evoked by the stimulus is estimated by  
87 convolving the neuronal population response and the canonical hemodynamic  
88 response function. In order to solve the under-constrained linear system, additionally,  
89 ridge regression regularization is used to enforce sparseness (see **Figure 1** below).  
90 The regularization technique suppresses noise and artifacts and thus allows our  
91 method to estimate the pRF topography more robustly.

92

93 The topographical methods do not force the pRF shape to have a certain parametric  
94 shape, and therefore can uncover the actual pRF structure. An appropriate  
95 parametric model can then be chosen based on the pRF topography. For example,  
96 the pRF topography can be used to separate the pRF center and surround, and then  
97 the subsequent pRF center modeling can be more accurate by minimizing the  
98 influence of surround suppression as well as the influence of other potential artifacts  
99 arising in areas distant to the pRF center. We have recently performed a quantitative  
100 comparison between our method and several other methods that directly (i.e. before  
101 estimating the topography) fit isotropic Gaussian<sup>1</sup>, anisotropic Gaussian, and  
102 difference of isotropic Gaussians to the pRF<sup>9</sup>. It was found that the topography-  
103 based method outperformed these methods with respect to pRF center modeling by  
104 achieving higher explained variance of the BOLD signal time series.

105

106 Accurate estimation of pRF properties in various areas reveals how they cover the  
107 visual field and is important for investigating the functional organization of the visual  
108 cortex particularly as it relates to visual perception. Properties such as how pRF size  
109 changes with eccentricity<sup>1,10</sup> and pRF center surround organization<sup>9</sup> are well studied  
110 in the human literature. The proposed method for estimating the pRF topography  
111 results in more accurate pRF parameter modelling and is more likely to reveal  
112 unknown regularities, not easily modeled a-priori in the direct parametric models.  
113 This approach will be especially suitable for studying pRF organization in patients  
114 with visual pathway lesions, for whom pRF structure is not necessarily predictable a-

115 priori. Below is described how to estimate the pRF topography and how to use the  
116 topography to model the pRF center.

117

## 118 **Protocol**

### 119 1. Data acquisition

120

121 1.1) Prepare a stimulus protocol that is effective in eliciting a reliable retinotopic  
122 visual response as previously described in Dumoulin and Wandell<sup>1</sup> and Lee et al.<sup>2</sup>.  
123 However, other well established paradigms are also applicable depending on the  
124 specific experimental question to be addressed.

125

126 1.2) Present bar stimuli drifting across the screen sequentially along 8 directions  
127 of space, in steps of 45 degrees. Ensure that the motion is in synchrony with scanner  
128 frame acquisition (TR~2sec) so that the bar moves a step once an fMRI frame starts  
129 and stays at the new location until the frame ends.

130

131 1.3) To measure a correct baseline signal, add epochs without bar stimulation<sup>1</sup>.

132

133 1.4)1. Define a field of view (10 to 15 degrees radius) in visual angle over which the  
134 stimulus is presented. Present moving or flickering checkerboard patterns (checker  
135 size = 0.94x0.94 deg<sup>2</sup>, pattern update rate = 250 msec/pattern) within the bar to elicit  
136 strong visual responses.

137

138 1.4)2. Input the following specific parameters: 8 evenly spaced directions of motion,  
139 bar width equal to 1.875 deg, and bars move by half the bar width per frame (2 sec).  
140 Additional details can be found in Lee et al.<sup>2</sup>.

141

142 1.4)3. Generate a spot (~0.25°) in the screen center on which the subject's eyes  
143 fixate during the experiment. Change color of the spot randomly in time.

144

145 1.5) Scan the brain of a subject in an MRI scanner using a typical echo-planar-  
146 imaging (EPI) scan that has 192 frames duration (24 frames in each direction of  
147 motion). Repeat the scans 4-8 times to increase signal-to-noise ratio.

148

149 1.6) Set parameters for the EPI sequence as follows: TR = 2sec, TE=40ms,  
150 matrix size = 64 x 64, 28 slices, voxel size = 3 x 3 x 3 mm<sup>3</sup>, flip angle = 90deg.,  
151 Alternatively, apply sequences with a finer resolution (e.g., 2 x 2 x 2 mm<sup>3</sup>) or a short  
152 TR (e.g., 1~1.5 sec) covering only the visual cortex<sup>2</sup>.

153

154 1.7) Track eye movements with an eyetracker system during functional scans to  
155 ensure fixation is maintained to within 1-1.5° of the fixation point. Note: Here, a head-  
156 coordinate based eyetracker in a goggle system is used, but other suitable  
157 eyetracker systems can be used instead.

158

159 1.8) Instruct the subjects to fixate the spot on the screen center generated in step  
160 1.3.2. To ensure the subjects are fixating, instruct them to report the color changes of  
161 the fixation spot.

162

163 1.9) Obtain anatomical scans, at 1x1x1 mm<sup>3</sup> resolution (e.g., T1-MPRAGE;  
164 TR=1900ms, TE=2.26ms, TI=900ms, flip angle = 9deg, 176 partitions). Note: These  
165 anatomical scans will be used for segmentation as well as for aligning the functional  
166 images to the anatomy both within and across scans. For better alignment between  
167 functional (EPI) images and the anatomy, obtain also an inplane anatomy scan, with  
168 resolution identical to the EPI, using T1-weighted fast spoiled gradient echo (SPGR)  
169 sequence<sup>1</sup>.

170

## 171 2. Data pre-processing

172

173 Note: Prior to estimating pRF properties, several typical fMRI data pre-processing  
174 steps are needed, such as head motion correction and alignment of functional  
175 volumes to the anatomical scan. In this article, all pre-processing, estimation,  
176 analysis and presentation of results obtained are performed using the open source  
177 MATLAB-based software toolbox VISTA LAB available on the VISTA software site.

178 [http://white.stanford.edu/newIm/index.php/Main\\_Page](http://white.stanford.edu/newIm/index.php/Main_Page).

179

180 2.1) Load the anatomical scan into MATLAB and prepare a volume anatomy  
181 using a function called createVolAnat.

182

183 2.2) Segment Gray matter, White matter, and CSF using the function “ItkGray”.

184

185 2.3) Prepare functional data by converting DICOM (**i.e., raw MRI file format for**  
186 **Siemens**) files into NIFTI (i.e., standard functional MRI file format) files, and load  
187 data into VISTA using a function called mrlnit.

188

189 2.4) Correct head-motion and align functional images to the anatomy loaded in  
190 step **2.1** using rxAlign based on an affine matrix transformation.

191

192 2.5) Average functional motion-corrected scans for improving signal-to-noise ratio  
193 by clicking mrVISTA → Analysis → TimeSeries → Average tSeries. Exclude from  
194 averaging scans during which eye movements deviates from fixation more than 1-  
195 1.5°. If signals from different runs have different dc-drifts, average functional scans  
196 after removing the dc-drifts.

197

198 2.6) Calculate the mapping coordinates between functional scans and Gray  
199 matter and identify corresponding Gray-matter voxels in the functional scans by  
200 selecting the following menus: mrVISTA → Window → Open Gray 3-View Window.  
201 Assign BOLD signals in the Gray matter voxels by interpolation, choosing one of the  
202 options available in mrVISTA.

203

204 3. Estimation of pRF topography and parametric modeling

205

206 3.1) **Download the code files through the following link**

207 <https://sites.google.com/site/leesangkyun/prf/codes.zip>, **extract the**

208 **compressed file** and place them in a preferred location of the local computer. Add  
209 the path of the folder in MATLAB.

210

211 3.2) Set the stimulus parameters used in the experiment by selecting the following  
212 menus: mrVISTA → Analysis → Retinotopic Model → Set Parameters. Specify the  
213 following parameters such as stimulus images, the stimulus size, the canonical  
214 hemodynamic function, the frame rate of the fMRI scanner.

215

216 3.3) Prior to the pRF estimation, prepare the initial parameter sets (Figure 1B).

217

218 3.3.1) Set the cross-validation sets in “tprf\_set\_params.m” from the code files. Divide  
219 timeseries into at least two subsets (one set for testing and the remaining sets for  
220 training) that are long enough for the bar to sweep the entire stimulus space.  
221 Alternatively, without averaging scans in step 2.4, validate scans by leaving out one  
222 scan for testing and using the remaining scans for training.

223

224 3.3.2) Set a coarse parameter set ( $\lambda$  in Figure 1;  $\lambda = [10^{-2} \ 10^{-1} \ 1 \ 10^1 \ 10^2]$ ) in  
225 “tprf\_set\_params.m”. Then, set a fine scale range ([0.1 0.3 0.5 0.7 0.9 1 3 5 7 9]) in  
226 “tprf\_set\_params.m”.

227

228 **Note:** The program uses the coarse set to select the  $\lambda$  resulting in the highest

229 explained variance. Then, the program searches the space around the selected  $\lambda$   
230 using the fine scale range, further refining the selection of  $\lambda$  that yields the highest  
231 explained variance.

232

233 3.3.3) Set a threshold (0.2) of the explained variance for visually responsive voxels in  
234 “tprf\_set\_params.m”. Note: This threshold is used as the reference for selection of  
235 visually responsive voxels. Alternatively, make an ROI for a non-visually responsive  
236 region (e.g., by drawing a sphere with a radius of 1cm in a non-visually responsive  
237 brain area), where the threshold can be automatically calculated.

238

239 3.3.4) Set a set of thresholds ([0.3, 0.5, 0.7]) for defining the pRF center region in the  
240 normalized topography in “tprf\_set\_params.m” (i.e., [0 to 1] or [-1 to 1] with epochs  
241 without bar stimulation in step 1.1.1).

242

243 Note: From the set of thresholds the program provided selects the “best” threshold,  
244 i.e. the threshold that defines a pRF central region for which the pRF center model  
245 explains the greatest signal variance. Alternatively, choose a different set of  
246 threshold values depending on the characteristics of the topography.

247

248 3.4) Execute “tprf\_runpRFest.m” from Supplemental Code Files to calculate the pRF  
249 topography (**Figure 1**) and fit a 2D anisotropic Gaussian. After specifying all  
250 parameters described in this protocol, and running the code, obtain the final  
251 estimation results.

252

253 [Figure 1 here]

254

### 255 **Representative Results:**

256 Accurate pRF modeling requires capturing pRF shapes correctly. Without knowing  
257 the pRF topography, the selection of circularly symmetric models used in prior  
258 studies<sup>1,9-11</sup> is a reasonable choice. This is because, if the local retinotopic  
259 organization is homogeneous in all directions of visual field, a local population  
260 response could be represented as a circularly symmetric cumulative aggregate of  
261 neuronal responses. However, our observations demonstrate that this is not  
262 necessarily the case (**Figure 2**). Therefore, observation of the pRF topography can  
263 be critical for selecting an appropriate parametric function for a pRF model. This is  
264 an advantage of the pRF topography, and so the topography-based models  
265 outperform the direct-fit isotropic Gaussian models in pRF center modeling, resulting  
266 typically in higher explained variance (**Figure 2**; see Lee et al.<sup>2</sup> for additional

267 comparisons with other models). These examples demonstrate the advantage of  
268 estimating the pRF topography prior to fitting the model.

269

270 [Figure 2 here]

271

272 One important requirement is to ensure that the fMRI paradigm used provides good  
273 retinotopy data. Then the pRF topography method can be used to estimate  
274 retinotopic eccentricity and azimuth maps (**Figure 3**). These maps show similar basic  
275 retinotopic architecture as previous methods<sup>1,4-7</sup>, but they are more accurate  
276 because observation of the pRF topography allows us to better separate the pRF  
277 center from the surround and from potential noise or artifacts distant to the pRF  
278 center. This, among other things, results in better estimation of the retinotopic maps  
279 at high eccentricities (a detailed account of the observed differences can be found in  
280 Lee et al.<sup>2</sup>).

281

282 [Figure 3 here]

283

284 The topography-based model (T-model) method can be used to estimate various  
285 pRF properties such as pRF size, elongation, orientation, and surround suppression  
286 efficiently, without having to test many different parametric models. To aid  
287 visualization of such properties, a MATLAB function (`tprf_plotpRF.m`) is provided that  
288 plots the pRF topography, the corresponding pRF center model, and their fit to the  
289 raw BOLD signal (**Figure 4**). Note that in some cases, pRF properties may also be  
290 estimated directly from the topography, eliminating the need for pRF modeling.

291

292 [Figure 4 here]

293

## 294 **Figures**

295

296 **Figure 1. pRF estimation process. (A)** Schematic illustration of the process  
297 followed for pRF topography estimation.  $h(t)$ : hemodynamic response function,  $A(t)$ :  
298 stimulus,  $m$ : pRF, Reg: L2-norm regularization. **(B)** Specific steps for pRF  
299 topography estimation and pRF center modeling. The set of parameters required for  
300 the estimation is listed in each step. A one-dimensional section of topography and its  
301 model are illustrated. Under “Model Fitting”, black and red curves represent the  
302 topography and its pRF center model with a center threshold of 0.5, respectively. The  
303 blue dashed line indicates a threshold for the pRF central region.

304



305 **Figure 2. Examples of pRF topography estimation and fit of pRF center models.**  
306 (A) A typical pRF topography. In the topography, red color indicates the most  
307 responsive area, which shows the pRF center lying on the middle right horizontal  
308 meridian. In the pRF topography, bar patterns across the pRF center structure with  
309 low weights are also sometimes observed. This relates to the fact that the area along  
310 the bar aperture passing through the pRF center is also stimulated simultaneously  
311 with the pRF center. They are easily eliminated in the thresholding step. (B)  
312 Comparison between a previous method (DIG; direct-fit isotropic Gaussian)<sup>1</sup> and  
313 topography-based pRF center model (T-model). The corresponding percent of  
314 explained variance is shown above each model. T-models show higher explained  
315 variance in all examples, with more accurate pRF shape capture. See Lee et al.<sup>2</sup> for  
316 more details and additional examples.

317

318 **Figure 3. Retinotopic maps and pRF size.** (A) Eccentricity and Polar angle maps  
319 in the left hemisphere of a subject. CS indicates the calcarine sulcus. In the right  
320 panel of Figure A, the black circle indicates a region-of-interest (ROI) from which the  
321 voxel whose pRF is illustrated in Figure 4 is taken. (B) Relationship between pRF  
322 size and eccentricity. The pRF size increases with eccentricity in visual areas V1-3.  
323 This plot is drawn from (A)

324

325 **Figure 4. Demonstration of the MATLAB toolbox developed by the authors.**  
326 This plot shows the pRF topography and corresponding pRF model fit of a voxel  
327 selected by a user. The illustrated voxel was selected from the ROI shown in **Figure**  
328 **3A**. *raw*: actual BOLD response, *pred<sub>i</sub>*: prediction with the pRF topography, *pred<sub>m</sub>*:  
329 prediction with the pRF center parametric model.

330

### 331 **Discussion**

332 This article demonstrates how to estimate the topography of visual population  
333 receptive fields in human visual cortex and how to use it to select an appropriate  
334 parametric model for the receptive field. For a successful retinotopy, an appropriate  
335 stimulation protocol and an efficient analysis method should be selected, and the  
336 subject's experimental parameters (motion and fixation) should be optimized. Bar  
337 stimuli moving sequentially across the visual field are an efficient stimulus paradigm  
338 for pRF estimation as it generates distinct BOLD responses from distinct stimulus  
339 locations. The provided method constructs the pRF topography. Since the problem of  
340 pRF estimation is generally under-determined, a mathematical tool called ridge  
341 regression<sup>3</sup> is used to enforce the reasonable constraint of sparseness on the pRF  
342 weight solution. This regularization technique is very effective at estimating the pRF

343 model when the number of observations (time points of the BOLD signal) is  
344 considerably smaller than the number of pixels covering the spatial dimension of the  
345 stimulus.

346

347 This method provides more robust estimation of the pRF center than previous  
348 methods. There are several reasons for this: 1) it first segments the pRF central  
349 region from the pRF topography and then fits an appropriate model, avoiding  
350 potential biases that may influence pRF model fits in direct models (i.e. surround  
351 suppression or noise artifacts far from the pRF center). 2) Having the ability to  
352 inspect the topography visually gives one the opportunity to validate the performance  
353 of the final model fit uncovering systematic errors, as well as 3) the possibility to  
354 detect features of the pRF structure that may otherwise go undetected. 4) By  
355 constraining the fitting area, this model is less likely to map the pRF inside the border  
356 of stimulus presentation incorrectly compared to direct fit models (see Figure 2B).  
357 Nonetheless, a user need be aware that the proposed method also has limitations  
358 for accurately capturing pRF shape near the stimulus border. This is due to the fact  
359 that near the border the bar stimuli activate partial receptive fields belonging to  
360 voxels whose pRF center would ordinarily be outside the stimulus presentation  
361 region. Any receptive field mapping method would be subject to this problem and  
362 show a relative peak at the border unless it can perfectly extrapolate from the part of  
363 the receptive field center that is mapped to the whole. Having said that, our method  
364 is more accurate than direct-fitting methods<sup>1,9</sup>, which tend to markedly overestimate  
365 the distance to the center of pRFs that lie near the stimulus presentation border (see  
366 Figures 5 and 6 of Lee et al.<sup>2</sup> for more detail).

367

368

369 As discussed, to construct a robust pRF topography depends on the free  
370 regularization parameter,  $\lambda$  (**Figure 1**), which can be optimized separately of  
371 individual voxels, or as a common parameter across all voxels. The regularization  
372 parameter influences pRF topography by adjusting the extent of fitting (over-fitting or  
373 under-fitting) to the data. While a small  $\lambda$  leads to noisy pRF topographies (i.e., over-  
374 fitting) compared to the actual pRF, a large  $\lambda$  suppresses visual responses and thus  
375 result in more spread topographies than justified by the actual pRF size (i.e., under-  
376 fitting). Selection of the optimal lambda is crucial for successful pRF estimation. We  
377 estimated  $\lambda$ 's in different subsets of data and evaluated these estimates using a  
378 cross-validation strategy. This minimizes biases in pRF topography estimation.  
379 Potential residual biases are further reduced in the pRF center modeling step, where

380 different topography thresholds are explored to select one that results in the highest  
381 explained variance (see Lee et al.<sup>2</sup>).

382

383 Finally, the topography approach proposed is computationally efficient. The  
384 estimation of pRF topographies over all voxels, including finding the optimal  
385 regularization parameter  $\lambda$ , takes only a few minutes in a PC environment.  
386 Identifying visually unresponsive voxels at this step excludes them from the more  
387 computationally demanding step of pRF-center modeling, further improving efficiency.  
388 Perhaps more importantly, investigators no longer need to test multiple different pRF  
389 models to find one that fits well, since they can be guided in choosing the  
390 appropriate model by the pRF topography.

391

392 The method demonstrated in this protocol measures population receptive field  
393 topography and uses it to guide population receptive field modeling. This approach  
394 reduces the bias present in direct population receptive field mapping methods,  
395 resulting in more robust and accurate pRF estimates. It also minimizes systematic  
396 errors and allows us to study the functional organization of the visual cortex with  
397 higher sensitivity. It is particularly applicable in the case of subjects with lesions of  
398 the visual pathways, in whom pRF structure may not be easy to anticipate a-priori.

399

#### 400 **Acknowledgments**

401 We thank the VISTA software group (Brian Wandell and associates, at Stanford).

402 S. S. was supported by McNair 2280403105, NEI R01-EY109272, and NEI R01-  
403 EY024019 and as HHMI Early Career Award. A. P. and G. K. was supported by the Max-  
404 Planck Society, G. K. was supported by the PLASTICISE project of the 7th Framework  
405 Programme of the European Commission, Contract no. HEATH-F2-2009-223524.

406

#### 407 **Disclosures**

408 The authors declare that they have no competing financial interests.

409

#### 410 **Reference**

411

- 412 1 Dumoulin, S. O. & Wandell, B. A. Population receptive field estimates in  
413 human visual cortex. *Neuroimage* 39, 647-660, doi:S1053-8119(07)00826-9  
414 [pii]  
415 10.1016/j.neuroimage.2007.09.034 (2008).
- 416 2 Lee, S., Papanikolaou, A., Logothetis, N. K., Smirnakis, S. M. & Keliris, G. A. A  
417 new method for estimating population receptive field topography in visual

418 cortex. *Neuroimage* 81, 144-157, doi:S1053-8119(13)00520-X [pii]  
419 10.1016/j.neuroimage.2013.05.026.

420 3 Hastie, T., Tibshirani, R. & Friedman, J. H. *The elements of statistical learning :  
421 data mining, inference, and prediction*. 2nd edn, (Springer, 2009).

422 4 Sereno, M. I. *et al.* Borders of multiple visual areas in humans revealed by  
423 functional magnetic resonance imaging. *Science* 268, 889-893 (1995).

424 5 Engel, S. A., Glover, G. H. & Wandell, B. A. Retinotopic organization in human  
425 visual cortex and the spatial precision of functional MRI. *Cereb Cortex* 7, 181-  
426 192 (1997).

427 6 Engel, S. A. *et al.* fMRI of human visual cortex. *Nature* 369, 525,  
428 doi:10.1038/369525a0 (1994).

429 7 DeYoe, E. A. *et al.* Mapping striate and extrastriate visual areas in human  
430 cerebral cortex. *Proc Natl Acad Sci U S A* 93, 2382-2386 (1996).

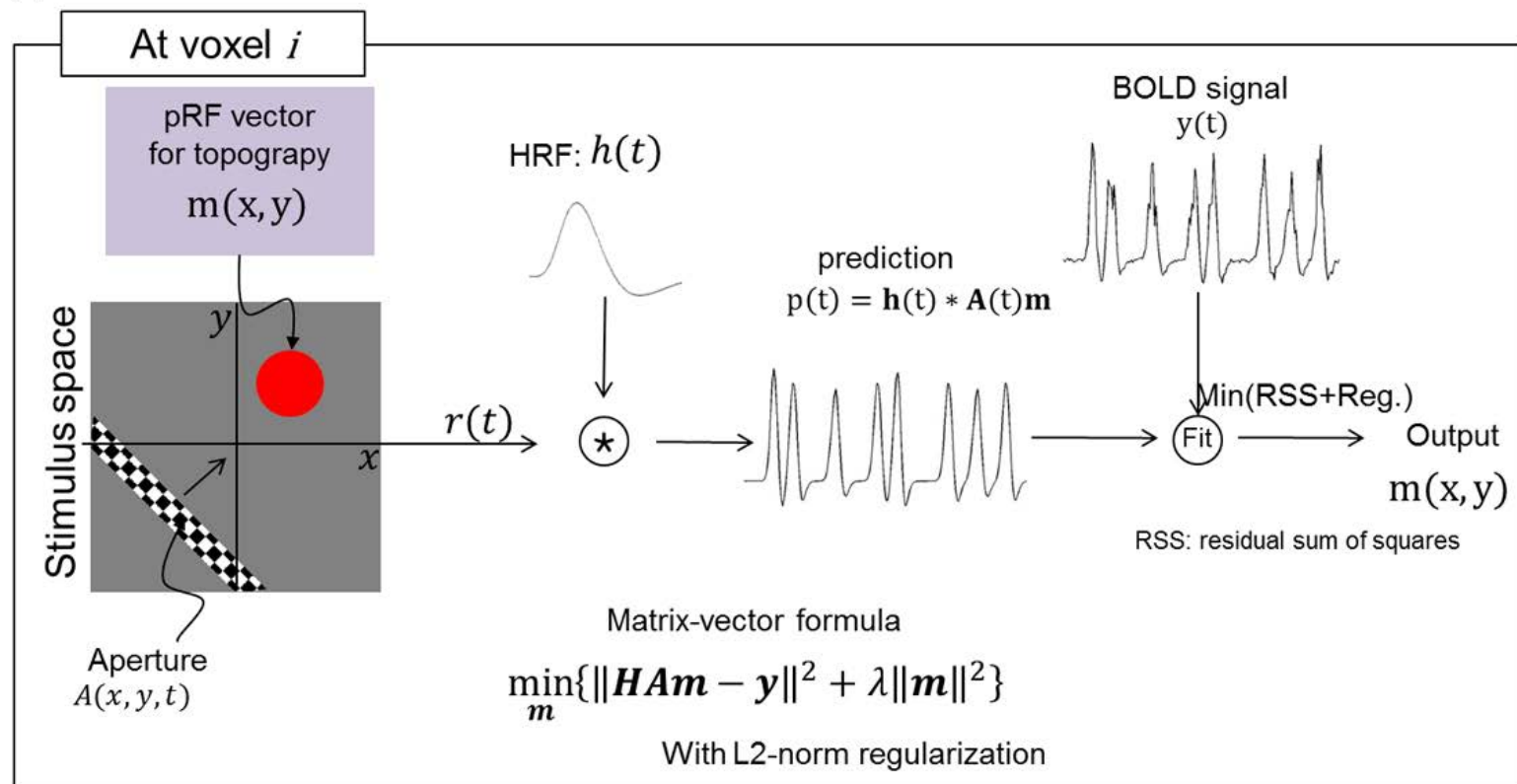
431 8 Greene, C. A., Dumoulin, S. O., Harvey, B. M. & Ress, D. Measurement of  
432 population receptive fields in human early visual cortex using back-projection  
433 tomography. *J Vis* 14, doi:14.1.17 [pii]  
434 10.1167/14.1.17.

435 9 Zuiderbaan, W., Harvey, B. M. & Dumoulin, S. O. Modeling center-surround  
436 configurations in population receptive fields using fMRI. *J Vis* 12,  
437 doi:10.1167/12.3.10  
438 10 [pii]  
439 12.3.10 [pii] (2012).

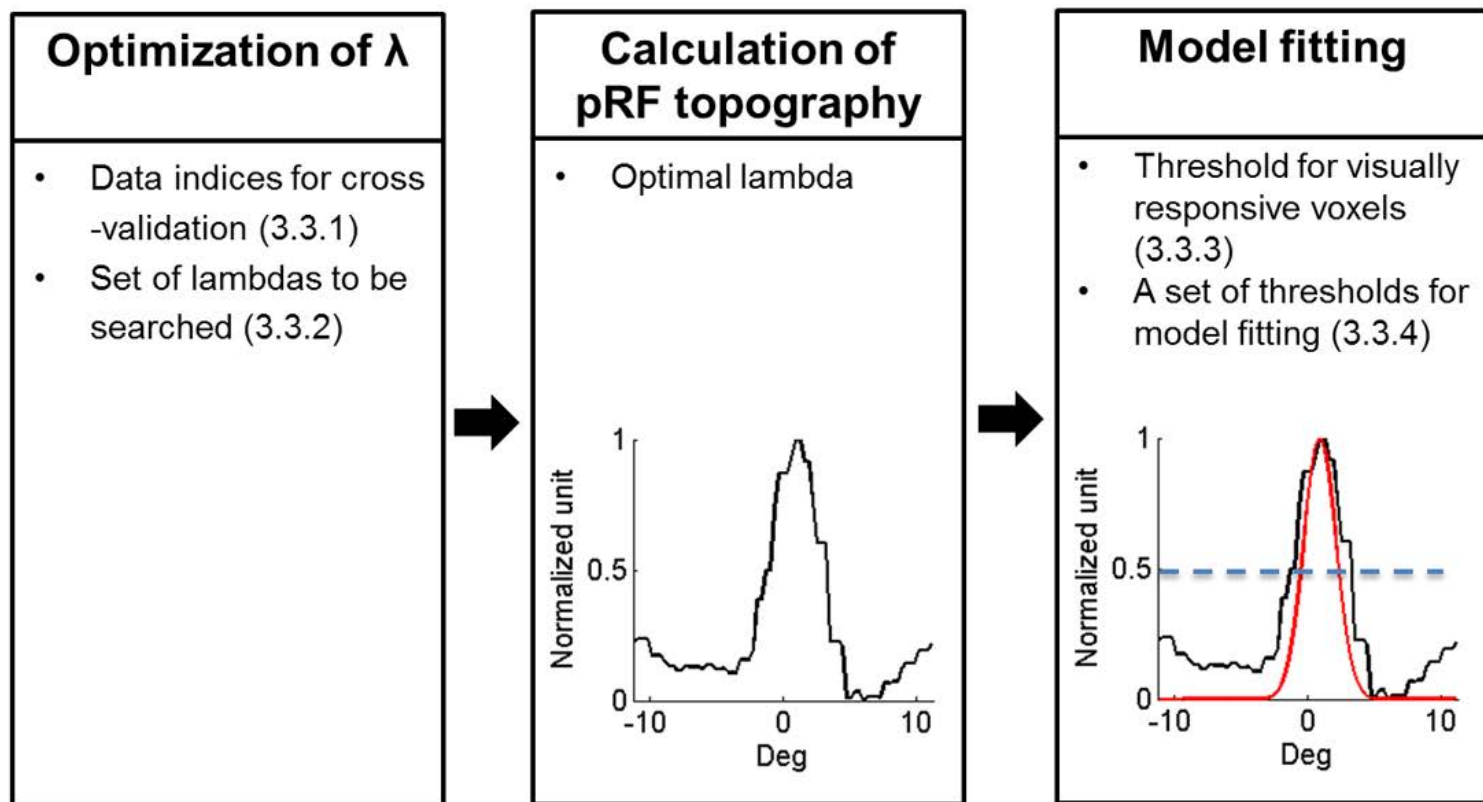
440 10 Harvey, B. M. & Dumoulin, S. O. The relationship between cortical  
441 magnification factor and population receptive field size in human visual cortex:  
442 constancies in cortical architecture. *J Neurosci* 31, 13604-13612,  
443 doi:31/38/13604 [pii]  
444 10.1523/JNEUROSCI.2572-11.2011 (2011).

445 11 Haak, K. V., Cornelissen, F. W. & Morland, A. B. Population receptive field  
446 dynamics in human visual cortex. *PLoS One* 7, e37686,  
447 doi:10.1371/journal.pone.0037686  
448 PONE-D-11-16437 [pii].  
449  
450

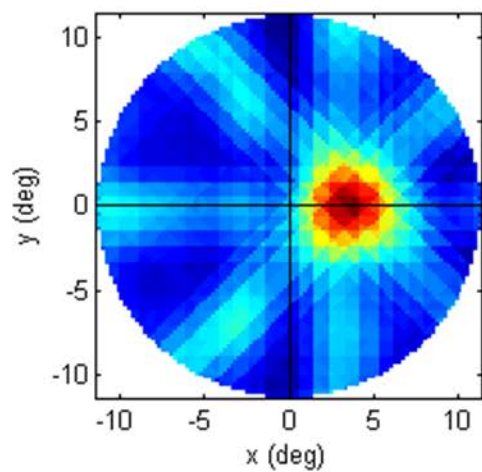
A



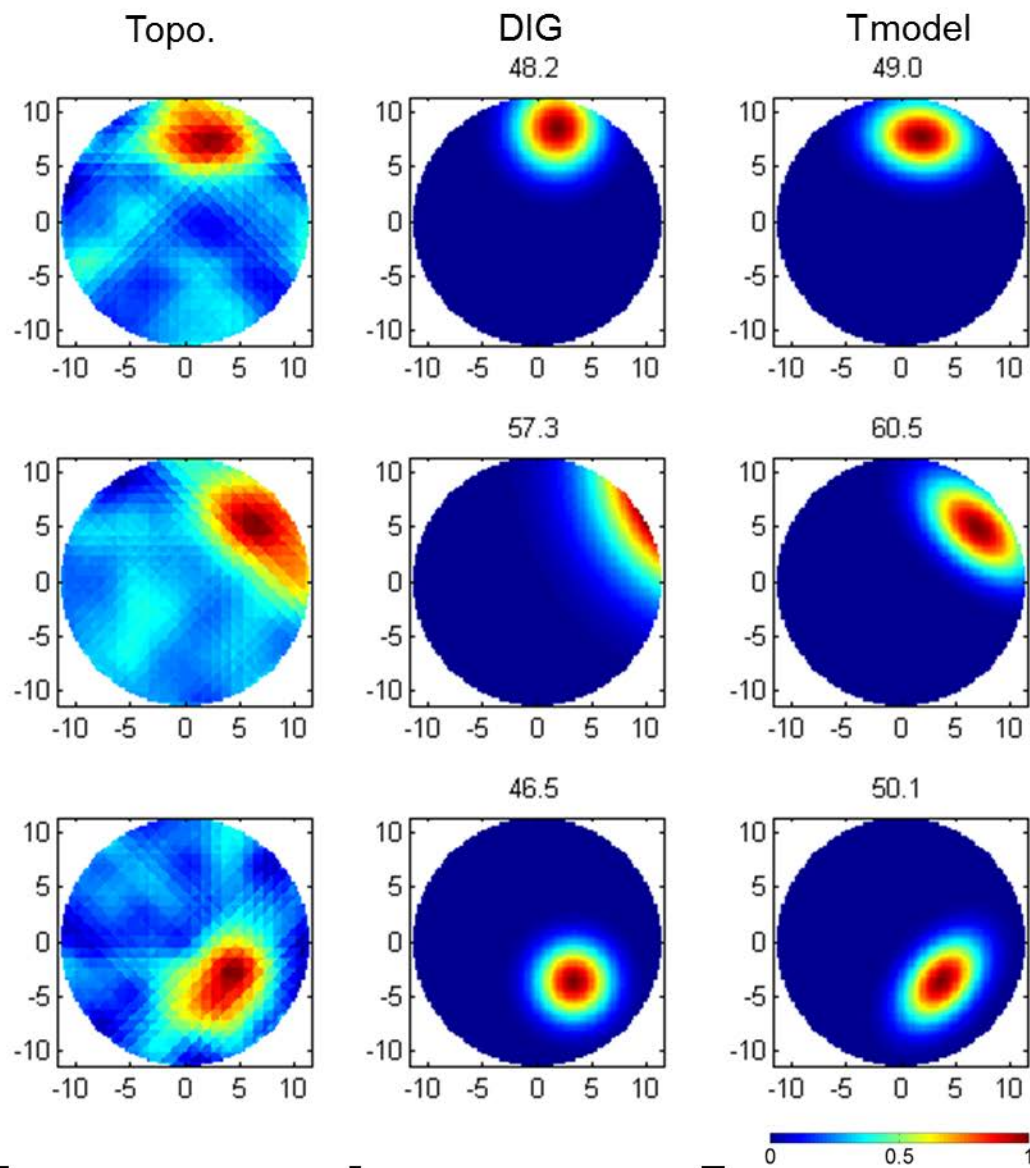
B



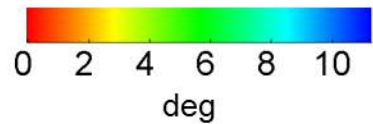
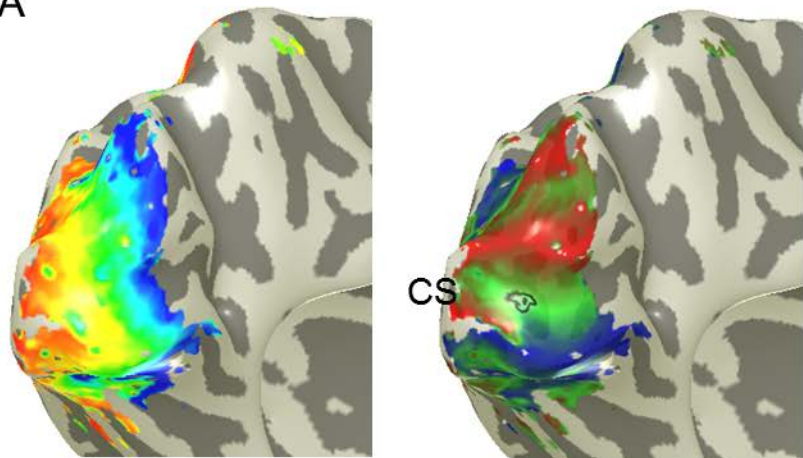
A



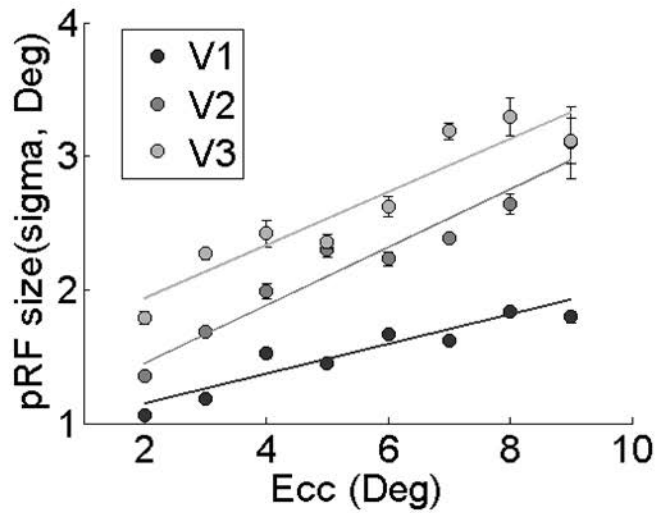
B



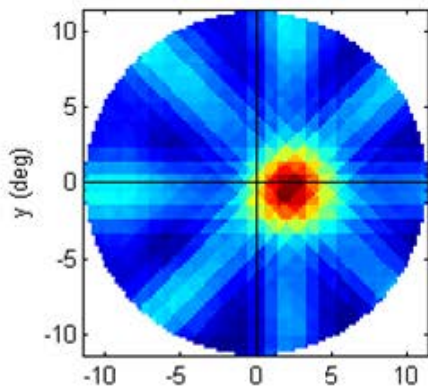
A



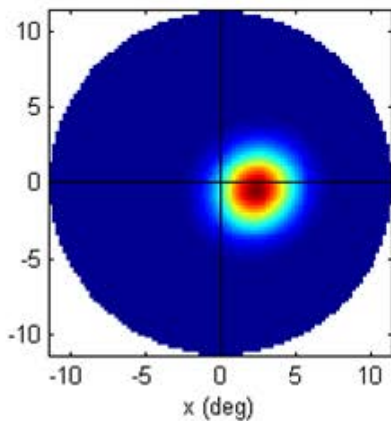
B



pRF topography



pRF model



Coords: [113 172 75]

Variance explained: 87.2% (Topo), 78.1% (Model)

$x=2.3, y=0.4$  (deg)

$r=2.3$  deg,  $\theta=80$  deg

$\sigma_1=1.7, \sigma_2=1.8,$   
 $\text{angle}=40.8$  deg

oval 2D pRF fit (x,y,si... ▾

Voxel:  | 16

